Chapter 1

Introduction

1.1 Overview

Vanadium dioxide (VO_2) is a transition → oxide with unique physical properties, making it a subject of intense research for several decades. Here's a brief history of VO_2 research till 2023:

1957: VO_2 was first discovered to undergo a semiconductor → metal transition (SMT), where it changes from a semiconducting material to a metallic material, upon heating.

1959: The first observation of the SMT in VO_2 was made by Morin at Bell Telephone Laboratories.

1960s-70s: The SMT in VO_2 was extensively studied, revealing its unique electronic and optical properties.

1980s-90s: The discovery of high temperature superconductivity in ceramics sparked renewed interest in VO_2, as a model system for studying electron-phonon (e-p) interactions.

2000s-2010s: Advances in thin-film deposition and nanoscale fabrication techniques allowed for the synthesis of VO_2-based devices with improved performance, leading to increased interest in potential applications in thermos electrics, memory devices, and optoelectronics.

2015: A team of researchers demonstrated the use of VO_2 as a switchable infrared (IR) reflector, opening up new possibilities for energy-efficient building materials.

Recent years (2017-2023): Continued research has focused on exploring the properties of VO_2 and its potential applications in various fields, including photonics, electronics, and energy conversion. The discovery of new materials with similar properties to VO_2, such as VO_2-based hetero-structures and vanadium oxides (VOs) with mixed valence states, has also expanded the scope of research in this area.

2021 and Beyond: The recent breakthroughs in the field of VO_2 research have paved the way for its potential use in a diverse array of applications, such as high-speed electronic devices, flexible electronics, and smart windows. Researchers are exploring new approaches to synthesizing high-quality VO_2 thin films with controlled crystal structure, in order to further optimize its properties and performance. The development of advanced fabrication and characterization techniques is also expected to fulfil a crucial role in ongoing efforts to unlock the full potential of VO_2 and its derivatives. Additionally, research is also being conducted on the integration of VO_2 with other materials, such as graphene and 2D (D: dimension)) materials, to create VO_2-based hetero-structures with improved properties and functionality. These hetero-structures have the potential to be used in a diverse array of applications, including high-speed data storage and processing, thermos electrics, and photonics.

Overall, the history of VO_2 research highlights the ongoing efforts to understand and harness the unique properties of this material, with the goal of advancing various fields of science and technology. The future of VO_2 research looks promising, with many opportunities for further discovery and innovation. With continued investment in this area, it is expected that VO_2 will fulfil an increasingly significant contribution in development of new technologies and materials, leading to breakthroughs in fields such as electronics, energy, and materials science.

1.2 VO_2: A Complex Mott Type Semiconductor

VO_2, a semiconductor (SC) of correlated $3d^1$ electrons (spin $s = ½$) near room temperature (RT). It is a transition metal oxide that is well-known as a "Mott type SC (insulator)," named after the British physicist Sir Nevill Mott. Mott SCs are materials that exhibit an SMT, meaning that they switch from being electrically semiconducting to conductive (metallic) state, based on changes in temperature or external stimuli [1–4]. In VO_2, this transition occurs at around 340 K, where it transforms from a semiconducting to metallic state, making it an ideal material for use in thermal switching devices and smart windows. In order to control the transition using external stimuli beyond temperature changes and for various applications, it is crucial to comprehend the material's behavior throughout the transition. Specifically, understanding the primary physical factor driving the transition is essential. The two primary explanations for the SMT in VO_2 that have been put out by the community are the one that views monoclinic VO_2 as a Peierls type SC and the one that views it as a Mott type SC. In the first scenario, the gap would open as a result of a structural alteration, namely pairing and the ensuing doubling of the cell [5, 6]. In the second scenario, the creation of the gap would be caused by the correlation of the electrons that were trapped in the narrow $d_{||}$ band after the shift of the π band [7]. In an effort to figure out this enigma, several research have been concluded. New intermediate phases and mixed behaviours have been added to the scenario as a consequence of theoretical calculations and experimental findings. One of the conclusions drawn to date is that categorizing VO_2 solely within one of the two scenarios is not feasible, as the behavior appears to be significantly more intricate. This is evidenced by the fact that neither the density functional theory (DFT) employing the local-density approximation (LDA) nor theories incorporating electron correlation, such as LDA+U, could fully

capture the experimental observations concerning the various phases of the material [8–10].

1.3 Significance of Resistive Switching

1.3.1 Hysteresis Width and Contrast

Both the width and contrast of the phase transition hysteresis are essential parameters to understanding the mechanics of the phase transition and designing effective devices. If the temperature at which a SC changes into a metal is denoted as point A in **Figure 1.1** and the temperature at which a metal changes into a SC is denoted as point B, then the hysteresis width is equal to the difference in temperature shown by $T_{SMT} - T_{MST}$. **Figure 1.1** shows that the optical contrast, the alteration in transmission or reflection, denoted by the letter C, is defined.

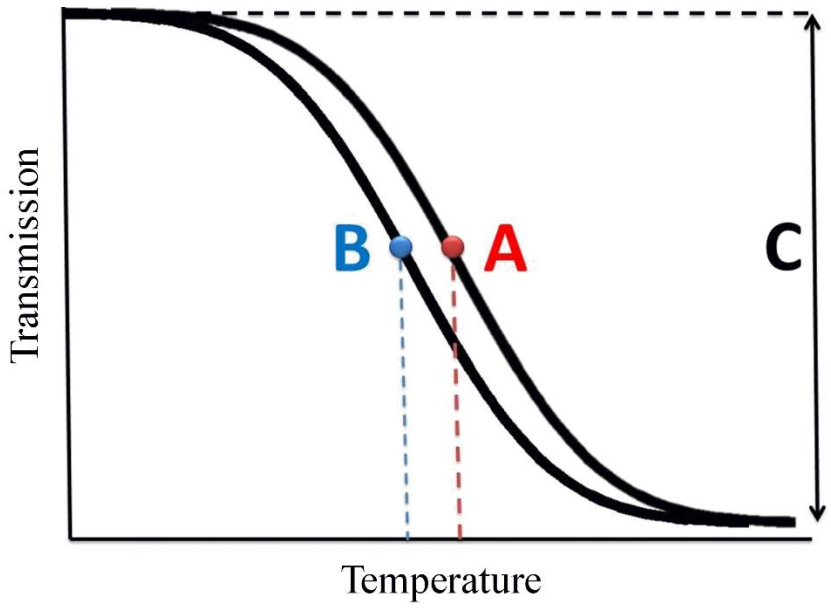

Figure 1.1 Schematic parameters associated during heating cooling thermal cycles.

The contrast is influenced by both the thickness (*t*) of the film and its composition. For a thin layer with uniformly spaced grains, each grain will have identical T_{SMT} and T_{MST}, and the resultant hysteresis will be narrow and resemble that of a single crystal. Taking into account a film that is formed of grains of two distinct sizes, we can say that each grain size will have its own T_{SMT} and T_{MST}. This film will have a hysteresis that is marginally broader than that of the film with the same grains but a different composition. One way to think about the hysteresis width is as a measurement of the grain homogeneity that exists across a film. Films that have a grain distribution that is narrow will have a hysteresis that is narrow, while films that have a grain distribution that is broad will have a hysteresis that is wide.

1.4 Literature Review

1.4.1 Magneli Phases of Vanadium Oxides

Vanadium has been demonstrated to exhibits multiple valence states, ranging from $V^{2+} \rightarrow V^{5+}$ to form vanadium oxygen complexes with multivalent oxides such as VO, V_2O_3, VO_2, and V_2O_5 [11, 12]. There are two forms of non-stoichiometric VOs that exhibit a phase transition response: one has a generic formula of V_nO_{2n+1} and exists between V_2O_5 to VO_2, and the second kind is referred to as the Magnéli type and has the general formula V_nO_{2n-1} [13, 14]. In contrast to the Magnéli family, V_nO_{2n+1} exhibits a reduced number of elements, such as V_3O_7 with a critical temperature (T_c) of 5.2 K and V_6O_{13} with an antiferromagnetic Néel temperature (T_N) of 155 K [15, 16]. However, V_nO_{2n-1} ($3 \leq n \leq 10$), which is based on the rutile VO_2 (R) structures of the Magnéli family, displays diverse T_c values as shown in **Figure 1.2** [14, 17]. Examples include V_8O_{15} (70 K), V_5O_9 (135 K), V_6O_{11} (170 K), V_4O_7 (250 K) and metallic V_7O_{13} [17].

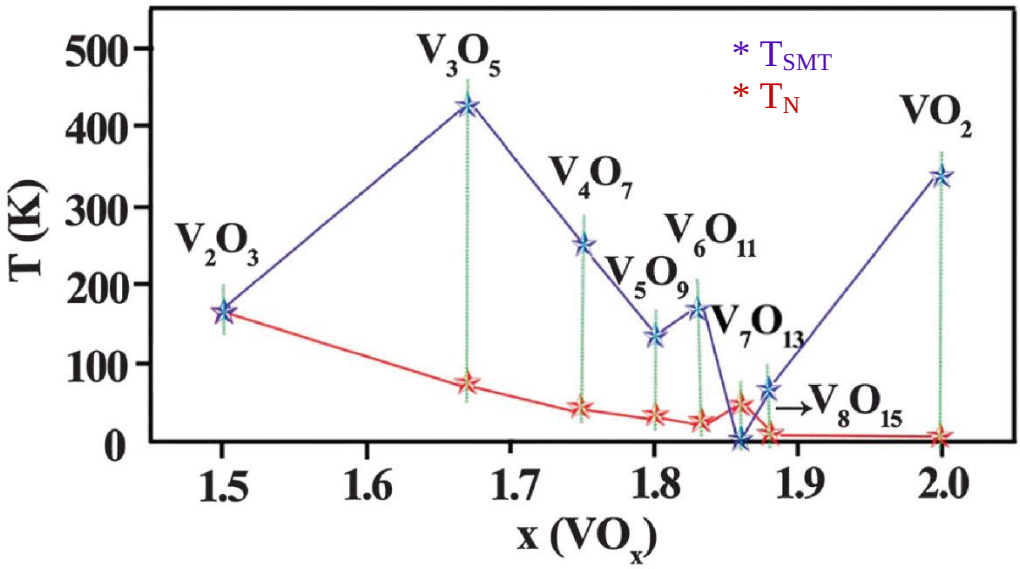

Figure 1.2 SMT and Néel temperatures in Magneli families [14].

1.4.2 Vanadium Dioxide

Multiple crystallographic phases exist for VO_2. These include the monoclinic or distorted rutile structure known as VO_2 (M), as well as the rutile (tetragonal) structure known as VO_2 (R). In addition, the physical parameter of VO_2 shows in **Table 1.1**. VO_2 has been identified in at least five metastable phases, which consist of the high temperature tetragonal phase VO_2 (A) (I4/m), the low temperature tetragonal phase VO_2 (A) (P4/ncc), the monoclinic phase VO_2 (B) (C2/m), the layer-structured VO_2 (C), and the recently characterized VO_2 (D) [18–20]. These polymorphs all have oxygen bcc lattices for their crystal structures, where the oxygen octahedra exhibit regularity, and the vanadium ions occupy the octahedral positions [20]. The phases most frequently observed in recent reports are shown in **Figure 1.3**, together with conditions that enable their transformation from one to another.

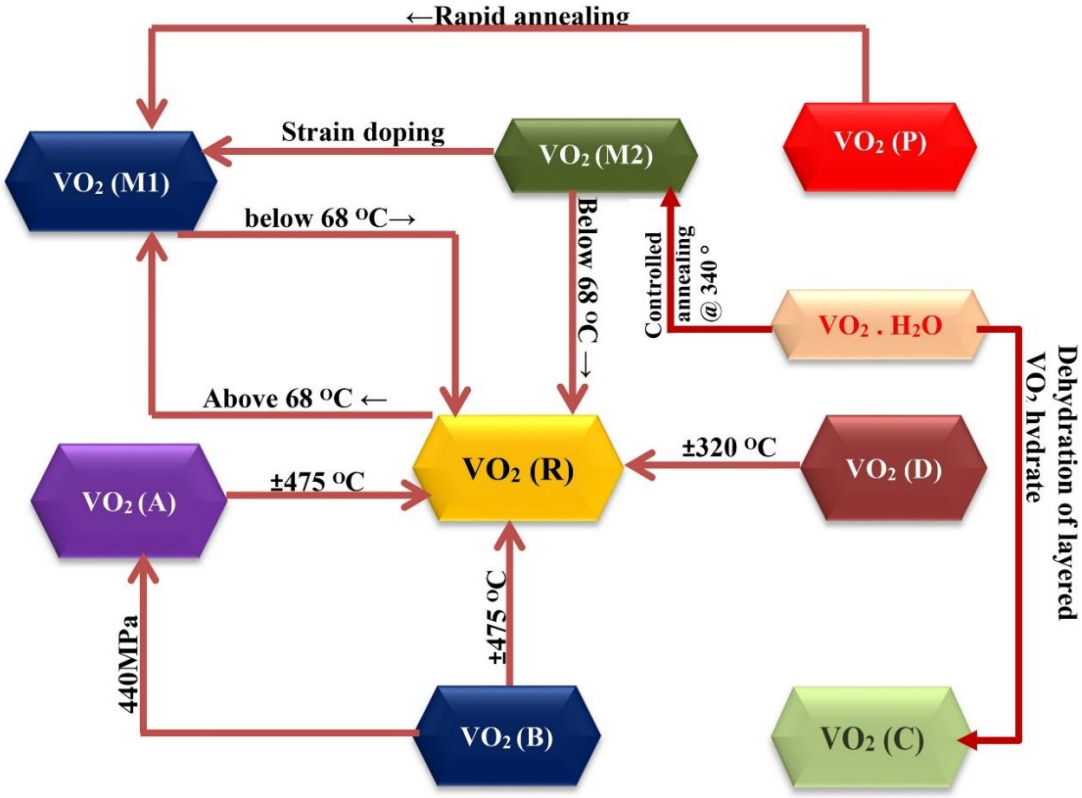

Figure 1.3 VO_2 phases and their conditions of transformation [21].

Only VO_2 (M/R), owing to changes in its crystallographic structure and electrical structure at 341 K and shows a completely first-order reversible SMT [22]. Every vanadium ion (V^{4+}) is situated at the center of an octahedron formed by six oxygen ions (O^{2-}) located at the vertices of the structure [23]. However, the phase transition is significantly influenced by factors such as crystallinity, divergence, and the size of VO_2. Morin discovered the existence of a reversible SMT in monoclinic VO_2 in 1959 [24]. VO_2 (M) belongs to the V_nO_{2n-1} (n = infinite) family and has been explored as a model material for clarifying 'e-e' interactions [25]. Upon elevating the temperature of VO_2 (M/R) beyond 341 K, a change in structure occurs, transitioning from the monoclinic SC (VO_2

(M)) phase (P21/c, M_1 phase, the most stable phase at RT) to the conducting rutile phase (VO_2 (R)) (P42/mnm, R phase). There is a dramatic shift in the optical characteristics of VO_2 (M/R) from IR and ultraviolet (UV) transmittance below SMT to IR and UV reflectance above SMT due to this phenomenon, which is called thermochromism [26, 27]. These optical alterations are connected with a change in resistivity that is about four to five orders of magnitude larger, yet the material nevertheless maintains its ability to transmit visible light [28, 29]. **Figure 1.4** depicts how the infinite linear chains of VO_2 (R) transform into the zigzag chains of VO_2 (M) that occur during the metal → semiconductor transition (MST) [30, 31]. Whether or not the outer 3d electrons of VOs are confined is determined by the intensities of the 'e-e' correlation for the cation-cation (V^{3+}-V^{3+} and V^{4+}-V^{4+} ions) interactions. According to Goodenough's findings, one may deduce from semi-empirical equations for critical separation value (R_c) for the 3d electron coupling interaction for vanadium ions is ≈ 2.93 [32]. Consequently, 3d electrons are mobile when the separation value (R) is less than the R_c, and localised when R is more than R_c. As an example, the VO_2 (M) zigzag chains create dimers of vanadium atoms at V-V distances of 0.316 nm (> R_c) and 0.262 nm (< R_c) along the c_R-axis, leading to SC behaviour and a resistance on the order of 0.1 Ω m (**Figure 1.4**) [33]. As the vanadium ions in VO_2 (R) form infinite chains with a V-V spacing of 0.288 nm (< R_c) along the c_R-axis, the d electrons are shared by all the ions in the same direction, resulting in a low resistivity of around 10^{-6} Ω m [34, 35].

Moreover, the phase transition can be induced by physical stress, electromagnetic wave, or electric field [36]. Due to its potential applications in sensors, energy-efficient thermochromic smart windows, switches, 4D imaging, energy storage devices, field-effect transitions, and more [37], VO_2 (M) has captured the attention of researchers. Factors such as size effect, interfacial strain, external strain, defects, stoichiometry,

doping, and others collectively contribute significantly to the solid-state SMT in VO_2 (M).

Table 1.1 Physical parameter of VO_2 at monoclinic and rutile crystal structure.

Property	Below T_c Value	Above T_c Value	Change	Reference
Crystal Structure	Monoclinic (M_1) P21/c	Rutile (R) P42/mnm	-	[38, 39]
Density	4.57 g/cm^3	4.65 g/cm^3	0.08 g/cm^3	[40]
Thermal Conductivity	3.5 W/(mK)	6.0 W/(mK)	2.5 W/(mK)	[41]
Heat Capacity	0.656 J/(gK)	0.78 J/(gK)	0.13 J/(gK)	[42]
Thermal Expansion Coefficient	-	-	4.87 x 10^{-6}/K	[43]
Latent Heat	-	-	51.8 J/g	[44]
Entropy	-	-	$(3.0\pm0.3)k_B$	[45]
Young's Modulus	140 GPa	140 GPa	-	[46]
Fracture Stress	5.20 GPa	5.2 GPa	-	[46]
Work Function	5.15 eV	5.30 eV	0.15 eV	[47]

VO_2 (M) is commonly produced by transforming VO_2 (B) and VO_2 (A) at elevated temperatures (823 K or higher) into VO_2 (M/R) [48–52]. However, achieving a pure phase of VO_2 (M) in a single step is notably challenging. As the VO_2 (R) phase convert into the stable VO_2 (M) phase upon cooling, both VO_2 (B) and VO_2 (A) can serve as precursors to generate VO_2 (R) through thermal treatment, albeit irreversibly. A hydrothermal process involving variations in pressure, temperature, and time can convert VO_2 (B) into VO_2 (A), with VO_2 (A) often identified as the intermediate phase during the transition from the metastable VO_2 (B) to the more stable VO_2 (R) phase [53, 54]. It has been a topic of discussion for quite some time as to what motivates the SMT. The Mott model proposes that the strong 'e-e' interaction is the driving force behind the limitation of electrons, which results in the formation of a Mott-Hubbard SC. However, according to

Peierl's model, the creation of a semiconducting phase is caused by lattice instability or structural distortions created by ‘e-p’ interactions [55, 56].

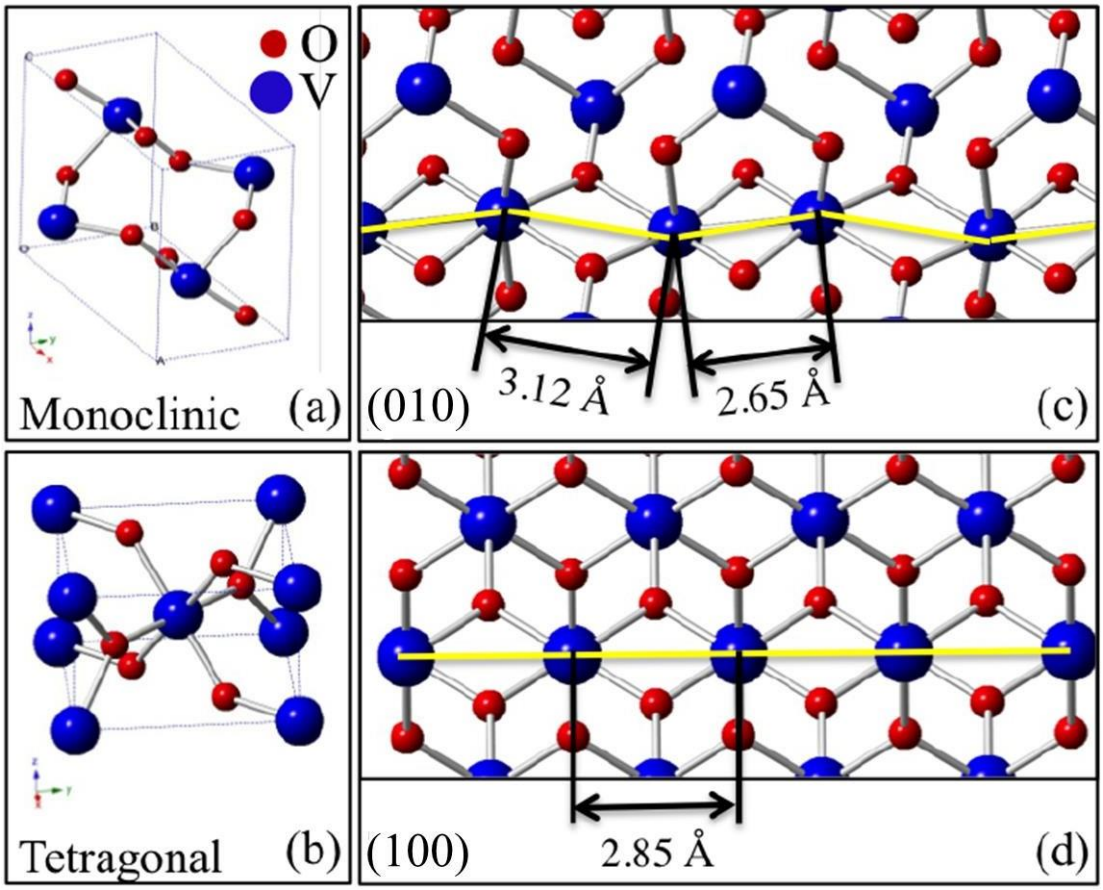

Figure 1.4 Crystal representations of (a) VO_2 (M) and (b) VO_2 (R). Perspectives along the c_R-axis of monoclinic (twisted V-V dimers) (c) and tetragonal (d) structures, respectively [30].

1.4.3 Peierls Structural Transition

Understanding the mechanism behind the phase shift by observing how the atoms rearrange themselves in VO_2 has been a topic of interest. The two main theories under examination are the Peierls and Mott-Hubbard models. According to the Peierls model, the instability of a 1-D chain of metal atoms (along the rutile c-axis) is what causes the structural transition since it has the potential to form dimers in a configuration with lower

energy. The Mott-Hubbard model relies on the contradiction arising from Coulomb repulsion and electronic correlation of the mobile electrons (hopping integral). Despite the fact that there are four phases known to exist (M_1, T, M_2, and R), most work only covers two (M_1 and R).

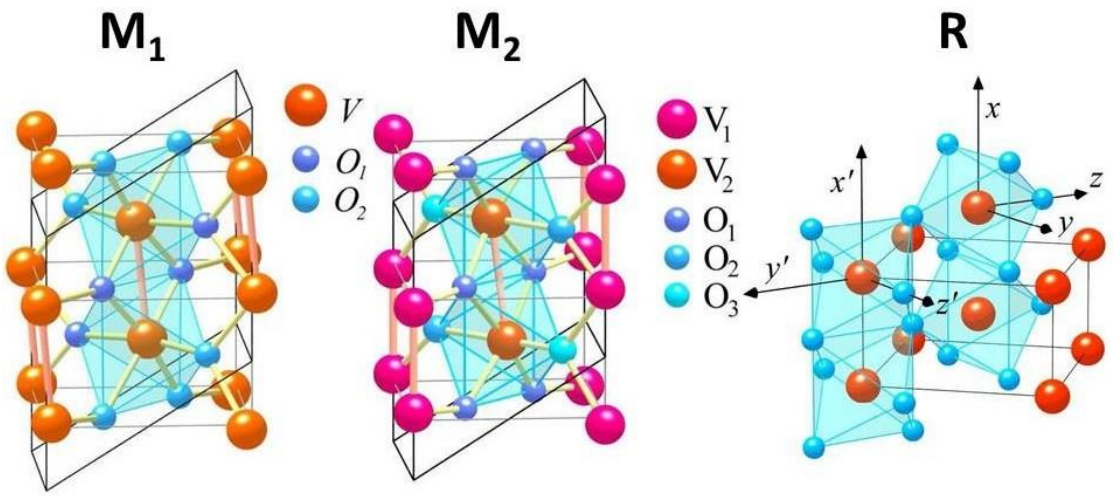

Figure 1.5 Atomic structure of VO_2 M_1, M_2 and R phase [57].

The atomic structure of the three most researched phases is shown in **Figure 1.5**. During the R phase, the locations of the metal and oxygen atoms are interchangeable with one another. In the M_2 phase, fifty percent of the vanadium atom chains exhibit dimerization along the c-axis (illustrated by purple atoms), while the remaining fifty is inclined along the c-axis (depicted by orange atoms), although they are still equally spaced apart. This results in three distinct habitats for the oxygen atoms to form bonds with one another. At the low-temperature final state, every vanadium atom has undergone dimerization and aligns along the c-axis. Additionally, there are distinct locations for the oxygen atoms, with lavender O_1 and blue O_2 indicating separate habitats.

1.4.4 Mott Electronic Transition

One explanation for the changes in band structure that occur at the Fermi energy as a consequence of the phase transition, as shown in **Figure 1.6**, was initially provided by Goodenough [58] and is still generally accepted today. In the illustration shown here, **Figure 1.6 (a)**, the octahedral crystal field created by the oxygen atoms separates the t_{2g} states into a $d_{||}$ state that is aligned along the rutile c-axis and the π^* states. When the vanadium atom is in the monoclinic form, the dimerization process separates the $d_{||}$ band into the bonding and antibonding states. In addition, the π^* band shifts to a higher energy state as a consequence of the dimerization, which causes a band gap of about ≈ 0.7 eV.

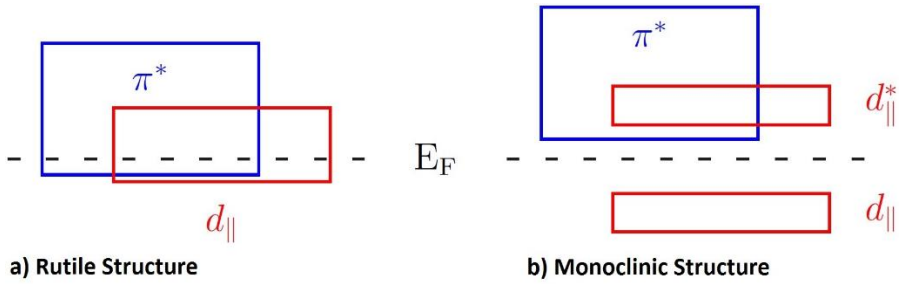

Figure 1.6 Band structure of VO_2 as described by Goodenough [57].

1.4.5 Triggering the Phase Transition

Heating is the easiest and most popular way to induce the phase change; in pure VO_2 films, the transformation takes place at 341 K. While Mott-Hubbard and Peierls processes both explain certain aspects of the transition, the Mott-Hubbard explanation seems to be more plausible in light of subsequent research [59, 60]. By establishing the metallic phase to far below ambient temperature, dopants like tungsten and molybdenum lower the phase

transition temperature. Nevertheless, this happens at the price of the electrical and optical contrast between the phases. The phase change may also be initiated by strain, which is most often done in single crystals [45, 61]. Cao et al. [61] first investigated the mechanics of strain in single crystals and drew a phase diagram, which subsequently improved by Park et al. [45]. Controlled strain has also been used to lower the phase transition temperature of VO_2 in thin films [62].

Multiple previous reports have long sought to induce the phase transition using an electric field [63–66]; nevertheless, there is still a lack of conclusive evidence for electric field switching. It might be challenging to differentiate if the applied field or Joule heating brought on by electric current is main causes the switching. Mostly, the electric field necessary to cause the phase change is approximately equal to the breakdown voltage. The electric field-induced phase transition seems to be significantly influenced by the Poole Frenkel (PF) effect, whereby an applied electric field enhances electron mobility [65, 66].

On other side, the mechanism involved in optical excitation by femtosecond pulses is quite different from the physics involved in thermal excitation. Optical excitation may start the phase change. According to Van Veenendaal et al. [67], the transition is kicked off by a photoinduced orbital imbalance between the $d_{||}$ and d_{π} bands, which then forces coherent motion of the vanadium dimers into the rutile phase. This is how the rutile phase is formed. According to Wall et al. [68], the coherent motion of the V-V dimers acts as an indication for the structural transition and is a significant driving factor in the phase change. This was discovered by observing the phase transition. Fluences of 7-10 mJ/cm^2 at 800 nm are often necessary to complete the phase change. Nevertheless, an increase in temperature may be employed to minimise the needed fluence, as shown by Pashkin et al. [69] and Cocker et al. [70]. The vast majority of ultrafast tests have been carried out

using light of 800 nm, which is more than twice as large as the optical band gap of 0.67 eV.

1.4.6 Phase Stability

Research on single crystals just recently revealed the precise parameters for the stability of the four VO_2 phases [45]. They plotted out the phase diagram (**Figure 1.7**) and observed a solid-state triple point where the M_1, M_2 and R phases coexisted by making electrical and optical measurements while meticulously regulating the strain and temperature of single crystal wires. Point T_c = 338 K, is where the triple point is discovered to exist. M_1, M_2 and R are three phases that may coexist.

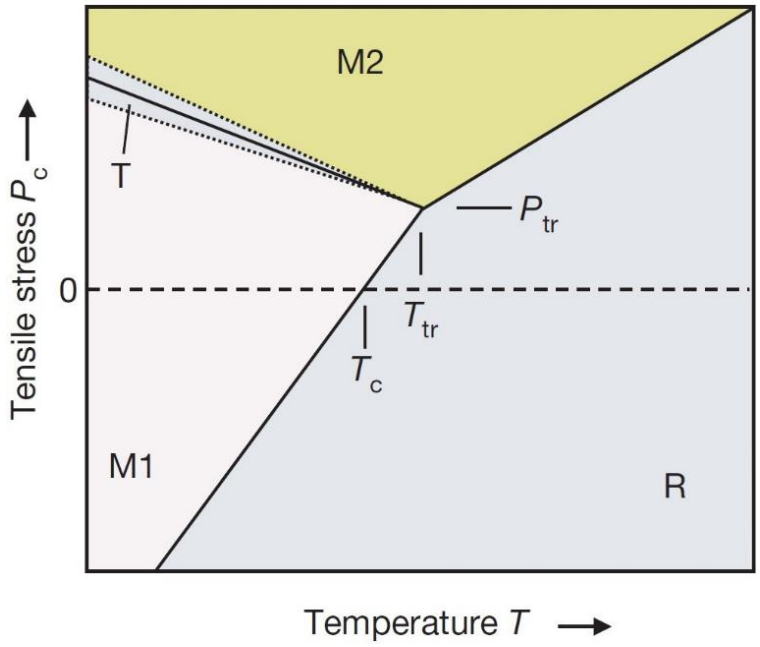

Figure 1.7 Phase diagram illustrating the impact of temperature stress on single crystals of VO_2 [45].

1.4.7 Semiconductor → Metal Transition Mechanism in VO_2

Understanding the nature of the SMT in VO_2 is a contemporary research concern [55, 56, 71]. Still, there is ongoing debate over the mechanics underlying phenomena. The SMT in VO_2 is thought to be caused by the interplay of spin, orbital dynamics, charge, and atomic structure. The Mott transition (strong 'e-e' interaction), the Peierls transition ('e-p' interaction), or both may be responsible for the phase change [31, 72–74]. Strong Coulombic repulsion between electrons is responsible for the SC phase, as shown by Warwick et al. [75] and Wentzcovitch et al. [55].

There has been a lot of research done on the band structure of VO_2 close to the Fermi level (E_F), and it has been shown that it is dominated by hybridization between the $3d^1$-V^{4+} and $2p^4$-O^{2-} orbitals [76–78]. There are five possible $3d^1$-V^{4+} states that may be hybridised together: d_{xy}, d_{xz}, d_{yz}, $d_{x^2-y^2}$ and d_{z^2}. Two of these orbitals, designated dxy and d_{z^2}, point in a straight direction towards oxygen atoms that are making higher energy σ bonds. As shown in **Figure 1.8**, in the metallic phase, the d levels of vanadium ions undergo splitting into higher-energy e_g states (empty) and lower-energy t_{2g} states [79].

Extensive examination has been conducted on the band structure of VO_2 in the vicinity of the E_F, primarily governed by the hybridization of the $3d^1$-V^{4+} and $2p^4$-O^{2-} orbitals [80–82]. Among the five available $3d^1$-V^{4+} states for hybridization (d_{xy}, d_{xz}, d_{yz}, $d_{x^2-y^2}$), two orbitals (dxy, d_{z^2}) directly point towards oxygen atoms, forming higher-energy σ bonds. Another pair of orbitals, denoted as d_{xz} and d_{yz}, are positioned between the oxygen atoms, resulting in lower-energy π bonds. The hybridization between the $3d^1$-V^{4+} orbitals and $2p^4$-O^{2-} orbitals lead to the splitting of both σ and π bonds into filled bonding states associated with $2p^4$-O^{2-} and anti-bonding states, σ* and π*, correlated with the $3d^1$–V^{4+}

orbital. Notably, the π* band is partially filled, while the higher-energy σ* band lies entirely above the E_F.

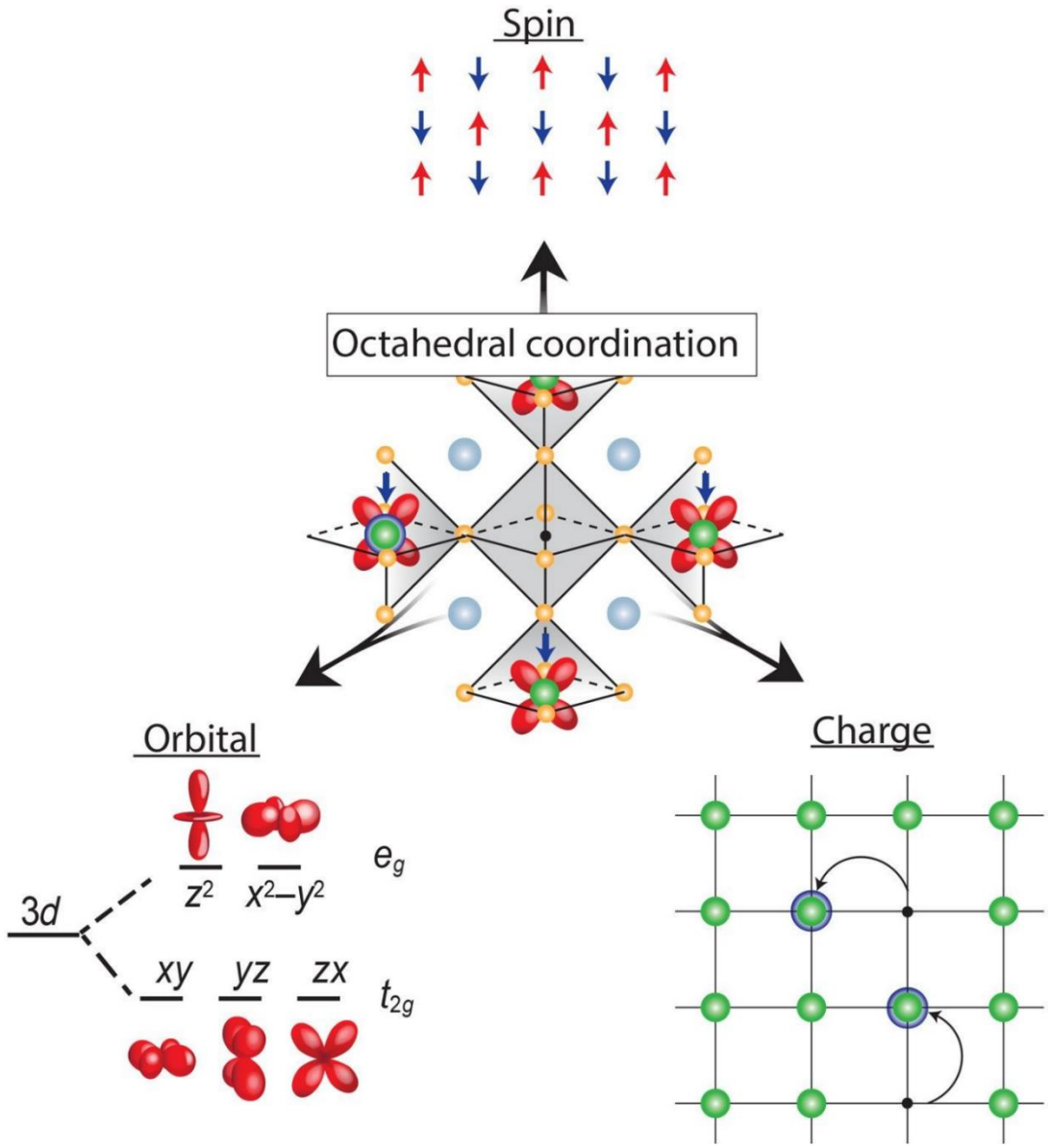

Figure 1.8 The octahedral arrangement of the V cation in various V_xO_y, phases, and the effect of coupling between the competing spin, charge, and orbital degrees of freedom on the optical and electronic properties in VOs [79].

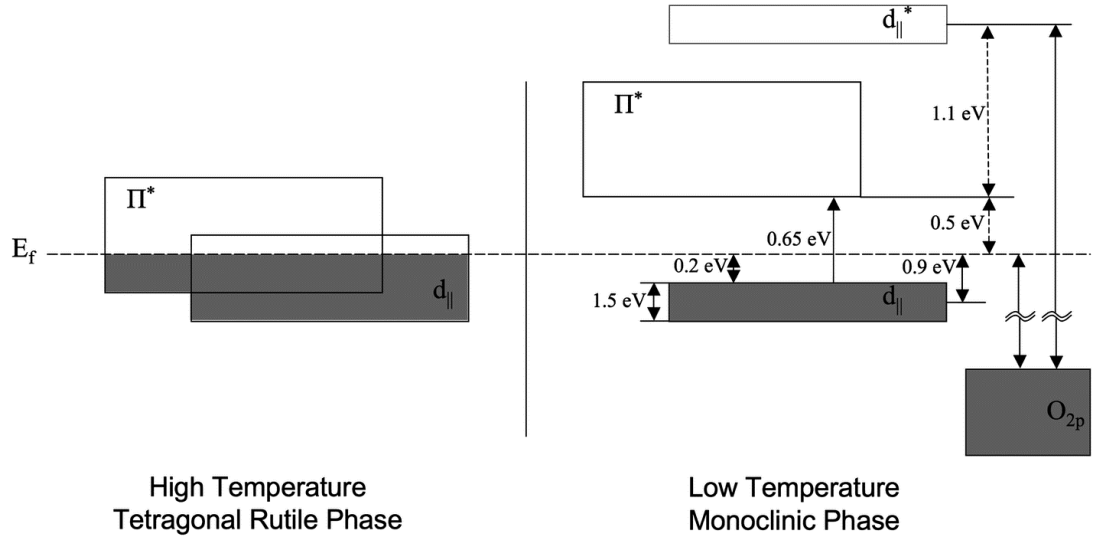

Figure 1.9 Diagram illustrating the schematic energy band structure of VO_2 [74].

The remaining $3d^1$-V^{4+} state is also a V-O π bond but is oriented along the asymmetric [001]R c_R-axis in the direction of the V-V chains. The asymmetry causes a decrease in the V-O hybridization, but an increase in V-V orbital overlap. This is a conducting band that is just half filled. When the V-V chain is distorted to the monoclinic lattice, it is broken into V-V dimers, that divide the $d_{||}$ band into full and empty states.

The $3d^1$-V^{4+}-$2p^4$-O^{2-} orbital overlap is also enhanced, which increases the separation of bonding and antibonding states. The enhanced band splitting raises the π* state over the E_F. The overall result is a band gap of around 0.65 eV [80–82]. **Figure 1.9** depicts the band diagrams for the rutile and monoclinic phases. The SMT or the structural change, respectively, are the cause and the outcome of the phase transition. Whether VO_2 is a Peierls or Mott type SC has been hotly contested for many years [80, 83–86]. In the case of the Peierls type SC, the structural transition causes the band splitting and the MST is the result. Hence, VO_2 would become a typical band SC. The band gap in a Mott type SC is brought on by 'e-e' correlations (Coulomb repulsion). VO_2 is generally accepted to be

a Mott type SC. The SMT occurs first, followed by the structural phase transition, according to femtosecond pump-probe observations in situ using temperature dependent x-ray diffraction (XRD) [76, 87].

1.4.8 Element Doping Effect in VO_2

The optical characteristics, SMT, and associated electrical transitions of VO_2 must be adjusted by stress, defects, grain size, or dopants in order for it to be employed for a variety of applications, including optical devices, sensors, and smart window coatings [77, 78, 88–90]. The elemental doping technique is one of them that is thought to be a successful method for regulating optical characteristics and lowering T_c of VO_2 [91]. Elemental doping may reduce VO_2's phase transition temperature to ambient temperature (298 K) for practical use in smart windows [92, 93]. Doping VO_2 with high-valent cations like Nb^{5+}, Mo^{6+}, Ta^{5+} and W^{6+} decreases the T_c point, whereas doping with large concentrations of low-valent cations like Al^{3+}, Cr^{3+}, Ti^{+4}, Ga^{3+} and Fe^{3+} raises the T_c point of VO_2 [28, 94, 95]. T_c may be shifted downward [96] with the use of low-valent cation doping at low concentrations. The SC phase instability and loss of V^{4+}-V^{4+} couples generated by Mo doping allowed Mai et al. [97] to reduce the SMT of VO_2 from 337 K to 315 K. A silicon-doped VO_2 film was employed by Zhang et al. [98] to reach a T_c of 326 K. T_c of 291 K was obtained by Zhang et al. [99] using N-doped samples like $VO_{1.87}N_{0.13}$ and $VO_{1.9}N_{0.1}$. The T_c of an Al-doped VO_2 sample may be decreased to 323 K and 313 K, respectively, as shown by Gentle et al. [100] and Chen et al. [101]. Using N-doped VO_2, Wan et al. [102] successfully lowered the T_c from 353 K to 336 K. Mg (0.3 at. %)-doped VO_2 was employed by Gagaoudakis et al. [103] to attain a typical low SMT at 322 K. For Ti (4 %)-doped VO_2, Chen et al. [104] attained a T_c of 324 K. For the Mg (7%)-doped VO_2, T_c was lowered by Mlyuka et al. [105] and Zhou et al. [106] from

337 K to 318 K and 341 K to 327 K, respectively. DFT studies by Wan et al. [107] showed that the E_g for C-doped VO_2 was the smallest (0.434 eV) compared to Mg, N, B and Al-doped VO_2 samples, suggesting that the T_c may be decreased more efficiently by doping with carbon. However, tungsten (W) has been identified experimentally as the most useful dopant for lowering the SMT of VO_2-based films to RT. Consequently, Mo, F and W are used to decrease T_c by 15 K, 20 K and 28 K at. %, respectively, and T_c may be dropped by 288 K, 292 K and 296 K per 1 at. % for Mo, F and W doping, respectively [107–112]. High-valent cation dopants like W^{6+} function as electron donors into the $3d^1$-V^{4+} valent band, which explains why W reduces the SMT of VO_2, and the loss of a homopolar V^{4+}-V^{4+} pair causes instability in the semiconducting structure of VO_2. T_c decreases as a consequence of these electron donation effects [113]. Doping also has an impact on the optical and thermochromic characteristics of VO_2. For instance, employing a magnetron sputtering method, VO_2 based films exhibit good switching when doped with Si [98]. By doping with Sn additions, Zhang et al. [114] also enhanced the thermochromic and optical properties of VO_2. The inclusion of dopants also affects the temperature-dependent parameters such as grain size, hysteresis width (the difference in T_c of the heating and cooling phase transition), and transmittance. For instance, Li et al. [115] were able to lower the hysteresis breadth of VO_2 from 291 K to 284 K in addition to improving the visual transmittance. By antimony doping, Gao and Yanfeng et al. [20] were able to regulate the shape, size, and polymorphology of VO_2 nanoparticles. Moreover, Liu et al. [116] showed that lanthanide doping allows for fine-tuning of the shape, size, and phase of $NaGdF_4$ nanocrystals (NCs). Doping VO_2 films, however, have not yet been thoroughly explored.

1.4.9 Application of VO_2

The thermochromic coating designed for what are commonly referred to as "smart windows" is one of the most fascinating applications that makes use of the SMT in VO_2. These later windows are coated with a substance that alters its optical characteristics based on temperature in order to decrease the amount of energy that is lost through the windows. Particularly, VO_2 changes from a phase that exhibits notable transparency in the visible spectrum and elevated reflectivity in the near-IR range at relatively high temperatures to a phase that has high transmittance in a large range that includes the visible and near-IR ranges when the temperature is low. This transition occurs when the temperature is relatively high. This would hinder the temperature in a room from decreasing too much during the winter and increasing too much during the summer, conserving energy [117, 118].

In addition, it is possible to create energy by directing the IR light that has been conveyed to lateral solar panels [119]. As a recording medium for holographic double-exposure interferometry in the femtosecond time domain [120], optical switches and fibres [121], scan lasers [122], bolometers [123, 124], nano-mechanical resonators [125], and micro actuators [126], VO_2 has also been employed. In addition to applications that are able to benefit from the sudden changes that take place in the optical and mechanical properties as a result of the transition, it is essential for the purpose of this thesis to briefly discuss the potential applications in electronics that can take advantage of the changes that take place in the transport characteristics of VO_2 during the phase shift.

Oxide electronics are promising possibilities for the succeeding era of products that get beyond Si-based electronics inherent limitations. Finding materials that combine the

benefits of volatile and non-volatile memories, such as static random-access memory and flash memories, is the electronics industry's key focus in particular.

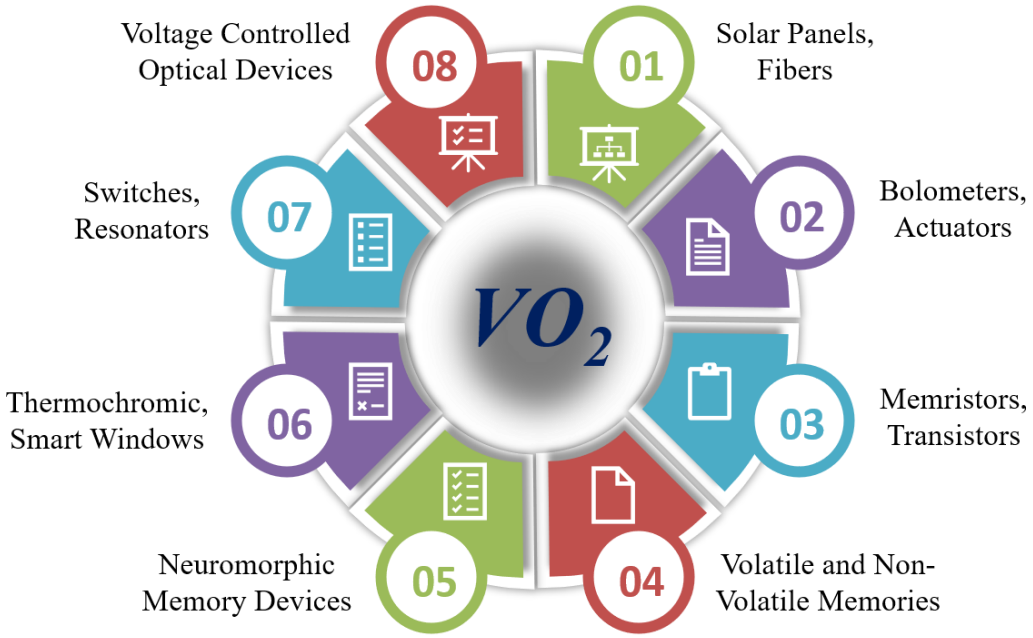

Figure 1.10 Depiction of VO_2 utilization in various field.

A class of inexpensive materials with simple scaling, quick programming, non-volatility, and low power consumption must be created for this purpose. Due to their ability to be manufactured at very low temperatures and then constructed in 3D stack structures, oxide-based devices may overcome conventional density restrictions. They can also be utilised to create quick, non-volatile, and energy-efficient electronics because to the fascinating physics behind the many phases they may acquire. For non-ohmic devices, threshold switching oxide devices, for instance, exhibit extremely close to perfect behaviour, essentially turning off completely for biases below the threshold voltage (V_{th}) and exhibiting minimal resistance for biases exceeding V_{th}. In these devices, NiO is employed as non-volatile memory and VO_2 is used as a selector, enabling quick

programming speed of tens of nanoseconds [127]. The advantages of utilizing VO_2 for electronic applications stem from its metallic "On state," which permits higher drive currents compared to SCs. Noteworthy features include its rapid transition, relatively low latent energy, full volume transition indicative of good scalability and reliability, and a potential metallic/semiconducting resistance ratio that can reach up to five orders of magnitude. The exception being nanoscale selectors [128]. Memristors [129] and two and three terminal field-effect transistor channels have both been constructed using VO_2. For devices with two terminals, a local Joule heating phenomenon is the main factor controlling the ON/OFF transition [130–132]. If the VO_2 channel current is relatively modest, the impact for three terminal devices should be solely electrostatic [133]. Several mechanisms, such as atomic ionization-induced charge doping or chemical reactions accompanied by a Mott transition, may be at play in this situation.

1.5 Memristor and It's Characteristics

In passive circuit theory, the three basic circuit elements are resistance, capacitance, and inductance. A basic circuit that links flux and charge was first presented in 1971 by University of California, Berkeley professor Leon O. Chua. This circuit is referred to as the absent fourth memristor element. In the end, a group at HP Labs under the direction of Stanley Williams found this elusive component in 2008 [134, 135]. According to research, a memristor is a non-linear, two-terminal passive electrical component whose conductance may be changed by adjusting the terminal voltages amplitude, direction, or duration. Memristors exhibit noteworthy properties, including strong compatibility with complementary metal-oxide SC technology, a compact device area conducive to high-density on-chip integration, non-volatility, rapid operation, low power dissipation, and significant scalability [136, 137]. Even though memristors were first developed as a

purely theoretical idea and then put into practice over a number of years, they are now widely used in fields including non-volatile random-access memory, machine learning, and neuromorphic computing [138, 139]. Moreover, owing to its robust computing and storage capabilities, the memristor stands out as a promising device for handling vast amounts of data and enhancing the efficiency of data processing in neural networks for artificial intelligence applications [140]. The correlation between key physical quantities (charge (q), voltage (v), flux (φ), and current (i)) and fundamental circuit elements (resistor (R), capacitor (C), inductor (L), and memristor (M)) is shown in **Figure 1.11 (A)** [134]. Specifically, capacitance (C) is characterized by a linear association between voltage and electric charge (C = dq/dv), inductance (L) involves a relationship between magnetic flux and current (L = dφ/di), and resistance (R) entails a relationship between voltage and current (R = dv/di). The memristor serves as the missing link between electric charge and flux, with its differential equation expressed as M = dφ/dq or equivalently G = dq/dφ. **Figure 1.11 (B)** shows the current-voltage characteristics of the memristor are distinguished by its fundamental identifier, the pinched hysteresis loop [141]. Unlike the I-V curves of basic elements such as R, C, and L, the memristor's I-V curve cannot be derived using these components. The shape of the pinched hysteresis loop allows for a rough classification into two types: digital memristors and analog memristors. In digital memristors, the resistance experiences a sudden change at higher resistance ratios, with both high-resistance and low-resistance states exhibiting a prolonged retention period, making them well-suited for memory and logic operations. On the other hand, analog memristors demonstrate a gradual change in resistance, making them more suitable for applications in analog circuits and hardware-based multi-state neuromorphic systems. The foundational pillars of system applications lie in the realm of memristor device technology and modelling research. At the apex of memristor's system applications,

including brain-machine interfaces, facial or image recognition, autonomous driving, edge computing for the Internet of Things, big data analytics, and cloud computing, is the theoretical circuitry illustrated in **Figure 1.11 (A)**. This diagram includes (A) the fundamental theoretical circuit components and (B) the characteristic pinched hysteresis I-V loop of memristor modelling and technology. Combining memristor-based digital, analogue, and memory circuits is essential to closing the gap between the applications of these device materials in complex systems and their actual use. Digital logic circuits, binary switches, and binary memory are the main applications for bistable memristors. Multi-state memristors, on the other hand, are useful for a variety of tasks. They can be used as essential parts of neuromorphic circuits, multi-bit memory, and reconfigurable analogue circuits.

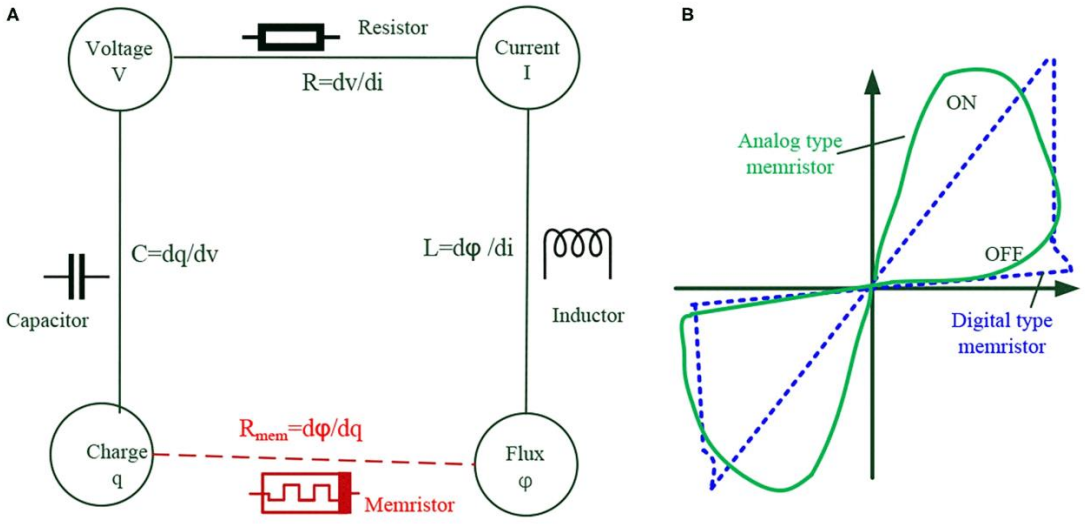

Figure 1.11 (A) Fundamental theoretical circuit components, and (B) pinched hysteresis I-V loop of the memristor [142].

REFRENCES

[1] B. Hong, K. Hu, Z. Tao, J. Zhao, N. Pan, X. Wang, M. Lu, Y. Yang, Z. Luo, and C. Gao, "Polymorph Separation Induced by Angle Distortion and Electron Delocalization Effect via Orbital Modification in VO_2 Epitaxial Thin Films," *Physical Review B,* **95** (2017) 075433 (8).

[2] S. Majid, D. K. Shukla, F. Rahman, S. Khan, K. Gautam, A. Ahad, S. Francoual, R. J. Choudhary, V. G. Sathe, and J. Strempfer, "Insulator-Metal Transitions in The *T* Phase Cr-Doped and *M1* Phase Undoped VO_2 Thin Films," *Physical Review B,* **98** (2018) 075152 (9).

[3] I. A. Mogunov, S. Lysenko, A. E. Fedianin, F. E. Fernández, A. Rúa, A. J. Kent, A. V. Akimov, and A. M. Kalashnikova, "Large Non-Thermal Contribution to Picosecond Strain Pulse Generation Using the Photo-Induced Phase Transition in VO_2," *Nature Communications,* **11** (2020) 1690 (8).

[4] J. Tadeo, D. Bhardwaj, D. Sheela, S. B. Krupanidhi, and A. M. Umarji, "Highly Photoresponsive VO_2 (M1) Thin Films Synthesized by DC Reactive Sputtering," *Journal of Materials Science: Materials in Electronics,* **31** (2020) 4687–4695.

[5] J. B. Goodenough, "The Two Components of The Crystallographic Transition in VO_2," *Journal of Solid State Chemistry,* **3** (1971) 490–500.

[6] R. M. Wentzcovitch, W. W. Schulz, and P. B. Allen, "VO_2: Peierls or Mott-Hubbard? A View from Band Theory," *Physical Review Letters,* **72** (1994) 3389–3392.

[7] A. Zylbersztejn, and N. F. Mott, "Metal-Insulator Transition in Vanadium Dioxide," *Physical Review B,* **11** (1975) 4383–4395.

[8] V. Eyert, "The Metal-Insulator Transitions of VO_2: A Band Theoretical Approach," *Annals of Physics,* **11** (2002) 650–702.

[9] A. Liebsch, H. Ishida, and G. Bihlmayer, "Coulomb Correlations and Orbital Polarization in The Metal-Insulator Transition of VO_2," *Physical Review B,* **71** (2005) 085109 (5).

[10] X. Yuan, Y. Zhang, T. A. Abtew, P. Zhang, and W. Zhang, "VO_2: Orbital Competition, Magnetism, and Phase Stability," *Physical Review B,* **86** (2012) 235103 (7).

[11] U. Begara, F. A. Crunteanu, and J. P. Raskin, "Raman and XPS Characterization of Vanadium Oxide Thin Films with Temperature," *Applied Surface Science,* **403** (2017) 717–727.

[12] S. Beke, "A Review of the Growth of V_2O_5 Films from 1885 to 2010," *Thin Solid Films,* **519** (2011) 1761–1771.

[13] N. Greenwood, and A. Earnshaw, "Chemistry of the Elements 2nd Edition" *Butterworth-Heinemann,* (1997).

[14] C. Wu, F. Feng, and Y. Xie, "Design of Vanadium Oxide Structures with Controllable Electrical Properties for Energy Applications," *Chemical Society Reviews*, **42** (2013) 5157–5183.

[15] K. Kosuge, T. Takada, and S. Kachi, "Phase Diagram and Magnetism of V_2O_3—V_2O_5 System," *Journal of the Physical Society of Japan*, **18** (1963) 318–319.

[16] A. Heidemann, K. Kosuge, Y. Ueda, and S. Kachi, "Hyperfine Interaction in V_3O_7," *Physica Status Solidi A*, **39** (1977) K37–K40.

[17] U. Schwingenschlögl, and V. Eyert, "The Vanadium Magnéli Phases V_nO_{2n-1}," *Annalen Der Physik*, **13** (2004) 475–510.

[18] R. Chen, L. Miao, C. Liu, J. Zhou, H. Cheng, T. Asaka, Y. Iwamoto, and S. Tanemura, "Shape-Controlled Synthesis and Influence of W Doping and Oxygen Nonstoichiometry on the Phase Transition of VO_2," *Scientific Reports*, **5** (2015) 14087 (12).

[19] L. Zhong, M. Li, H. Wang, Y. Luo, J. Pana, and G. Li, "Star-Shaped VO_2 (M) Nanoparticle Films with High Thermochromic Performance," *CrystEngComm*, **17** (2015) 5614–5619.

[20] Y. Gao, C. Cao, L. Dai, H. Luo, M. Kanehira, Y. Dingd, and Z. L. Wang, "Phase and Shape Controlled VO_2 Nanostructures by Antimony Doping," *Energy and Environmental Science*, **5** (2012) 8708–8715.

[21] V. T. Lukong, K. Ukoba, and T. C. Jen, "Fabrication of Vanadium Dioxide Thin Films and Application of Its Thermochromic and Photochromic Nature in Self-Cleaning: A Review," *Energy and Environment*, **34** (2023) 3495–3528.

[22] S. Liang, Q. Shi, H. Zhu, B. Peng, and W. Huang, "One-Step Hydrothermal Synthesis of W-Doped VO_2 (M) Nanorods with a Tunable Phase-Transition Temperature for Infrared Smart Windows," *ACS Omega*, **1** (2016) 1139–1148.

[23] A. Rúa, R. D. Díaz, S. Lysenko, and F. E. Fernández, "Semiconductor-Insulator Transition in VO_2 (B) Thin Films Grown by Pulsed Laser Deposition," *Journal of Applied Physics*, **118** (2015) 125308 (10).

[24] F. Morin, "Oxides Which Show a Metal-to-Insulator Transition at the Neel Temperature," *Physical Review Letters*, **3** (19591) 34–36.

[25] B. Hu, Y. Zhang, W. Chen, C. Xu, and Z. L. Wang, "Self-Heating and External Strain Coupling Induced Phase Transition of VO_2 Nanobeam as Single Domain Switch," *Advanced Materials*, **23** (2011) 3536–3541.

[26] B. Blackburn, M. J. Powell, C. E. Knapp, J. C. Bear, C. J. Carmalt, and I. P. Parkin, "$[\{VOCl_2(CH_2(COOEt)_2)\}_4]$ as a Molecular Precursor for Thermochromic Monoclinic VO_2 Thin Films and Nanoparticles," *Journal of Materials Chemistry C*, **4** (2016) 10453–10463.

[27] Y. Chen, S. Zhang, F. Ke, C. Ko, S. Lee, K. Liu, B. Chen, J. W. Ager, R. Jeanloz, V. Eyert, and J. Wu, "Pressure-Temperature Phase Diagram of Vanadium Dioxide," *Nano Letters*, **17** (2017) 2512–2516.

[28] Z. Liang, L. Zhao, W. Meng, C. Zhong, S. Wei, B. Dong, Z. Xu, L. Wan, and S. Wang, "Tungsten-Doped Vanadium Dioxide Thin Films as Smart Windows with Self-cleaning and Energy-Saving Functions," *Journal of Alloys and Compounds*, **694** (2017) 124–131.

[29] Y. Ma, H. Zhou, J. Zhu, S. Ji, S Bao, R. Li, and P. Jin, "Synthesis of Flake-Like VO_2 (M) by Annealing a Novel $(NH_4)_{0.6}$ V_2O_5 Phase and Its Thermochromic Characterization," *Ceramics International*, **42** (2016) 16382–16386.

[30] H. Asayesh-Ardakani, A. Nie, P. M. Marley, Y. Zhu, P. J. Phillips, S. Singh, F. Mashayek, G. Sambandamurthy, K. B. Low, R. F. Klie, S. Banerjee, G. M. Odegard, and R. S. Yassar, "Atomic Origins of Monoclinic-Tetragonal (Rutile) Phase Transition in Doped VO_2 Nanowires," *Nano Letters*, **15** (2015) 7179–7188.

[31] S. Biermann, A. Poteryaev, A. I. Lichtenstein, and A. Georges, "Dynamical Singlets and Correlation-Assisted Peierls Transition in VO_2," *Physical Review Letters*, **94** (2005) 026404 (4).

[32] J. B. Goodenough, "Anomalous Properties of the Vanadium Oxides," *Annual Review of Materials Science*, **1** (1971) 101–138.

[33] C. Everhart, and J. MacChesney, "Anisotropy in the Electrical Resistivity of Vanadium Dioxide Single Crystals," *Journal of Applied Physics*, **39** (1968) 2872–2874.

[34] M. Liu, H. Y. Hwang, H. Tao, A. C. Strikwerda, K. Fan, G. R. Keiser, A. J. Sternbach, K. G. West, S. Kittiwatanakul, J. Lu, S. A. Wolf, F. G. Omenetto, X. Zhang, K. A. Nelson, and R. D. Averitt, "Terahertz-Field-Induced Insulator-to-Metal Transition in Vanadium Dioxide Metamaterial," *Nature*, **487** (2012) 345–348.

[35] E. Strelcov, Y. Lilach, and A. Kolmakov, "Gas Sensor Based on Metal-Insulator Transition in VO_2 Nanowire Thermistor," *Nano Letters*, **9** (2009) 2322–2326.

[36] S. C. Hong, M. Lee, and D. Kim, "The Optical Behavior of VO_2 Film Modulated by the Morphology and Preferred Growing Axis," *Bulletin of the Korean Chemical Society*, **38** (2017) 85–90.

[37] Y. Ke, X. Wen, D. Zhao, R. Che, Q. Xiong, and Y. Long, "Controllable Fabrication of Two-Dimensional Patterned VO_2 Nanoparticle, Nanodome, and Nanonet Arrays with Tunable Temperature-Dependent Localized Surface Plasmon Resonance," *ACS Nano*, **11** (2017) 7542–7551.

[38] S. Westman, "Note on a Phase Transition in VO_2," *Acta Chemica Scandinavica*, **15** (1961) 217–217.

[39] G. Anderson, "Studies on Vanadium Oxides," *Acta Chemica Scandinavica*, **10** (1956) 623–628.

[40] H. Wen, L. Guo, E. Barnes, J. H. Lee, D. A.Walko, R. D. Schaller, J. A. Moyer, R. Misra, Y. Li, E. M. Dufresne, D. G. Schlom, V. Gopalan, and J. W. Freeland, "Structural and Electronic Recovery Pathways of a Photoexcited Ultrathin VO_2 Film," *Physical Review B*, **88** (2013) 165424 (8).

[41] D. W. Oh, C. Ko, S. Ramanathan, and D. G. Cahill, "Thermal Conductivity and Dynamic Heat Capacity across the Metal-Insulator Transition in Thin Film VO_2," *Applied Physics Letters*, **96** (2010) 151906 (3).

[42] C. N. Berglund, and H. J. Guggenheim, "Electronic Properties of VO_2 Near the Semiconductor-Metal Transition," *Physical Review*, **185** (1969) 1022–1033.

[43] D. Kucharczyk, and T. Niklewski, "Accurate X-Ray Determination of The Lattice Parameters and The Thermal Expansion Coefficients of VO_2 Near the Transition Temperature," *Journal of Applied Crystallography*, **12** (1979) 370–373.

[44] M. K. Liu, M. Wagner, E. Abreu, S. Kittiwatanakul, A. McLeod, Z. Fei, M. Goldflam, S. Dai, M. M. Fogler, J. Lu, S. A. Wolf, R. D. Averitt, and D. N. Basov, "Anisotropic Electronic State via Spontaneous Phase Separation in Strained Vanadium Dioxide Films" *Physical Review Letters*, **111** (2013) 096602 (5).

[45] J. H. Park, J. M. Coy, T. S. Kasirga, C. Huang, Z. Fei, S. Hunter, and D. H. Cobden, "Measurement of a Solid-State Triple Point at The Metal-Insulator Transition in VO_2," *Nature*, **500** (2013) 431–434.

[46] H. Guo, K. Chen, Y. Oh, K. Wang, C. Dejoie, S. A. S. Asif, O. L. Warren, Z. W. Shan, J. Wu, and A. M. Minor, "Mechanics and Dynamics of the Strain-Induced M1-M2 Structural Phase Transition in Individual VO_2 Nanowires," *Nano Letters*, **11** (2011) 3207–3213.

[47] C. Ko, Z. Yang, and S. Ramanathan, "Work Function of Vanadium Dioxide Thin Films across the Metal-Insulator Transition and the Role of Surface Nonstoichiometry," *ACS Applied Materials and Interfaces*, **3** (2011) 3396–3401.

[48] J. C. Valmalette, and J. R. Gavarri, "High Efficiency Thermochromic VO_2 (R) Resulting from the Irreversible Transformation of VO_2 (B)," *Materials Science and Engineering: B*, **54** (1998) 168–173.

[49] H. Zhang, Q. Li, B. Cheng, K. Xu, L. Lan, S. Zhao, Y. Li, T. Cui, and B. Liu, "A Facile Method to Control the Diameter of Monoclinic Vanadium Dioxide Rods," *Journal of Nanoscience and Nanotechnology*, **17** (2017) 2791–2795.

[50] B. Dong, N. Shen, C. Cao, Z. Chen, H. Luo, and Y Gao, "An Intermediate Phase $(NH_4)_2V_4O_9$ and Its Effects on the Hydrothermal Synthesis of VO_2 (M) Nanoparticles," *CrystEngComm*, **18** (2016) 558–565.

[51] Z. Song, L. Zhang, F. Xia, N. A. S. Webster, J. Song, B. Liu, H. Luoae, and Y. Gao, "Controllable Synthesis of VO_2 (D) and their Conversion to VO_2 (M) Nanostructures with Thermochromic Phase Transition Properties," *Inorganic Chemistry Frontiers*, **3** (2016) 1035–1042.

[52] S. R. Popuri, M. Miclau, A. Artemenko, C. Labrugere‖, A. Villesuzanne, and M. Pollet, "Rapid Hydrothermal Synthesis of VO_2 (B) and Its Conversion to Thermochromic VO_2 (M1)," *Inorganic chemistry*, **52** (2013) 4780–4785.

[53] Y. Zhang, X. Tan, C. Huang, and C. Meng, "Hydrothermal Treatment with VO_2 (B) Nanobelts for Synthesis of VO_2 (A) and W Doped VO_2 (M) Nanobelts," *Materials Research Innovations*, **19** (2015) 295–302.

[54] A. Srivastava, H. Rotella, S. Saha, B. Pal, G. Kalon, S. Mathew, M. Motapothula, M. Dykas, P. Yang, E. Okunishi, D. D. Sarma, and T. Venkatesan, "Selective Growth of Single Phase VO_2 (A, B, and M) Polymorph Thin Films," *APL Materials*, **3** (2015) 026101 (10).

[55] R. M. Wentzcovitch, W. W. Schulz, and P. B. Allen, "VO_2 Peierls or Mott-Hubbard? A View from Band Theory," *Physical Review Letters*, **72** (1994) 3389–3392.

[56] T. Rice, H. Launois, and J. Pouget, "Comment on VO_2: Peierls or Mott-Hubbard? A View from Band Theory," *Physical Review Letters*, **73** (1994) 3042–3042.

[57] V. Eyert, "The Metal-Insulator Transitions of VO_2: A Band Theoretical Approach," *Annals Phys (Leipzig)*, **11** (2002) 650–704.

[58] J. B. Goodenough, "The Two Components of the Crystallographic Transition in VO_2," *Journal of Solid State Chemistry*, **3** (1971) 490–500.

[59] V. R. Morrison, R. P. Chatelain, K. L. Tiwari, A. Hendaoui, A. Bruhcs, M. Chaker, and B. J. Siwick, "A Photoinduced Metallike Phase of Monoclinic VO_2 Revealed by Ultrafast Electron Diffraction," *Science*, **346** (2014) 445–448.

[60] J. Laverock, S. Kittiwatanakul, A. A. Zakharov, Y. R. Niu, B. Chen, S. A. Wolf, J. W. Lu, and K. E. Smith, "Direct Observation of Decoupled Structural and Electronic Transitions and an Ambient Pressure Monoclinic-Like Metallic Phase of VO_2," Physical Review Letters, **113** (2014) 216402 (5).

[61] J. Cao, Y. Gu, W. Fan, L. Q. Chen, D. F. Ogletree, K. Chen, N. Tamura, M. Kunz, C. Barrett, J. Seidel, and J. Wu, "Extended Mapping and Exploration of the Vanadium Dioxide Stress-Temperature Phase Diagram," *Nano Letters*, **10** (2010) 2667–2673.

[62] N. B. Aetukuri, A. X. Gray, M. Drouard, M. Cossale, L. Gao, A. H. Reid, R. Kukreja, H. Ohldag, C. A. Jenkins, E. Arenholz, K. P. Roche, H. A. Durr, M. G. Samant, and S. S. P. Parkin, "Control of the Metal-Insulator Transition in Vanadium Dioxide by Modifying Orbital Occupancy," *Nature Physics*, **9** (2013) 661–666.

[63] H. T. Kim, B. G. Chae, D. H. Youn, G. Kim, K. Y. Kang, S. J. Lee, K. Kim, and Y. S. Lim, "Raman Study of Electric-Field-Induced First-Order Metal-Insulator Transition in VO_2 Based Devices," *Applied Physics Letters*, **86** (2005) 242101 (3).

[64] D. Ruzmetov, K. T. Zawilski, V. Narayanamurti, and S. Ramanathan, "Structure-Functional Property Relationships in RF-Sputtered Vanadium Dioxide Thin Films," *Journal of Applied Physics*, **102** (2007) 113715 (7).

[65] B. A. Kruger, A. Joushaghani, and J. K. S. Poon, "Design of Electrically Driven Hybrid Vanadium Dioxide (VO_2) Plasmonic Switches," *Optics Express*, **20** (2012) 23598–23609.

[66] P. Markov, R. E. Marvel, H. J. Conley, K. J. Miller, R. F. Haglund Jr., and S. M. Weiss. "Optically Monitored Electrical Switching in VO_2," *ACS Photonics*, **2** (2015) 1175–1182.

[67] M. V. Veenendaal, "Ultrafast Photoinduced Insulator-to-Metal Transitions in Vanadium Dioxide," *Physical Review B,* **87** (2013) 235118 (6).

[68] S. Wall, D. Wegkamp, L. Foglia, K. Appavoo, J. Nag, R. F. Haglund Jr, J. Stähler, and M. Wolf, "Ultrafast Changes in Lattice Symmetry Probed by Coherent Phonons," *Nature Communications,* **3** (2012) 721 (6).

[69] A. Pashkin, C. Kübler, H. Ehrke, R. Lopez, A. Halabica, R. F. Haglund Jr., R. Huber, and A. Leitenstorfer, "Ultrafast Insulator-Metal Phase Transition in VO_2 Studied by Multiterahertz Spectroscopy," *Physical Review B,* **83** (2011) 195120 (9).

[70] T. L. Cocker, L. V. Titova, S. Fourmaux, G. Holloway, H. C. Bandulet, D. Brassard, J. C. Kieffer, M. A. E. Khakani, and F. A. Hegmann, "Phase Diagram of the Ultrafast Photoinduced Insulator-Metal Transition in Vanadium Dioxide," *Physical Review B,* **85** (2012) 155120 (11).

[71] M. M. Qazilbash, M. Brehm, B. G. Chae, P. C. Ho, G. O. Andreev, B. J. Kim, S. J. Yun, A. V. Balatsky, M. B. Maple, F. Keilmann, H. T. Kim, and D. N. Basov, "Mott Transition in VO_2 Revealed by Infrared Spectroscopy and Nano-Imaging," *Science,* **318** (2007) 1750–1753.

[72] M. W. Kim, W. G. Jung, H. Cho, T. S. Bae, S. J. Chang, J. S. Jang, W. K. Hong, and B. J. Kim, "Substrate-Mediated Strain Effect on the Role of Thermal Heating and Electric Field on Metal-Insulator Transition in Vanadium Dioxide Nanobeams," *Scientific Reports,* **5** (2015) 10861 (10).

[73] J. P. Pouget, H. Launois, J. P. D'Haenens, P. Merenda, and T. M. Rice "Electron Localization Induced by Uniaxial Stress in Pure VO_2," *Physical Review Letters,* **35** (1975) 873–875.

[74] J. P. Pouget, H. Launois, T. M. Rice, P. Dernier, A. Gossard, G. Villeneuve, and P. Hagenmuller, "Dimerization of a Linear Heisenberg Chain in the Insulating Phases of $V_{1-x}Cr_xO_2$," *Physical Review B,* **10** (1974) 1801–1815.

[75] M. E. Warwick, and R. Binions, "Advances in Thermochromic Vanadium Dioxide Films," *Journal of Materials Chemistry A,* **2** (2014) 3275–3292.

[76] H. T. Kim, Y. W. Lee, B. J. Kim, B. G. Chae, S. J. Yun, K. Y. Kang, K. J. Han, K. J. Yee, and Y. S. Lim, "Monoclinic and Correlated Metal Phase in VO_2 as Evidence of the Mott Transition: Coherent Phonon Analysis," *Physical Review Letters,* **97** (2006) 266401(4).

[77] G. Pan, J. Yin, K. Ji, X. Li, X. Cheng, H. Jin, and J. Liu, "Synthesis and Thermochromic Property Studies on W Doped VO_2 Films Fabricated by Sol-Gel Method," *Scientific Reports,* **7** (2017) 6132 (10).

[78] L. Kang, Y. Gao, and H. Luo, "A Novel Solution Process for the Synthesis of VO_2 Thin Films with Excellent Thermochromic Properties," *ACS Applied Materials and Interfaces,* **1** (2009) 2211–2218.

[79] M. Brahlek, L. Zhang, J. Lapano, H. T. Zhang, R. E. Herbert, N. Shukla, S. Datta, H. Paik, and D. G. Schlom, "Opportunities in Vanadium-Based Strongly Correlated Electron Systems," *MRS Communications,* **7** (2017) 27–52.

[80] J. B. Goodenough, "The Two Components of the Crystallographic Transition in VO_2," *Journal of Solid State Chemistry*, **3** (1971) 490–500.

[81] N. B. Aetukuri, A. X. Gray, M. Drouard, M. Cossale, L. Gao, A. H. Reid, R. Kukreja, H. Ohldag, C. A. Jenkins, E. Arenholz, K. P. Roche, H. A. Dürr, M. G. Samant and S. S. P. Parkin, "Control of the Metal-Insulator Transition in Vanadium Dioxide by Modifying Orbital Occupancy," *Nature Physics*, **9** (2013) 661–666.

[82] S. Chen, X. J. Wang, L. Fan, G. Liao, Y. Chen, W. Chu, L. Song, J. Jiang, and C. Zou, "The Dynamic Phase Transition Modulation of Ion-Liquid Gating VO_2 Thin Film: Formation, Diffusion, and Recovery of Oxygen Vacancies," *Advanced Functional Materials*, **26** (2016) 3532–3541.

[83] H. T. Stinson, A. Sternbach, O. Najera, R. Jing, A. S. Mcleod, T. V. Slusar, A. Mueller, L. Anderegg, H. T. Kim, M. Rozenberg, and D. N. Basov, "Imaging the Nanoscale Phase Separation in Vanadium Dioxide Thin Films at Terahertz Frequencies," *Nature Communications*, **9** (2018) 3604 (9).

[84] A. Cavalleri, T. Dekorsy, H. H. W. Chong, J. C. Kieffer, and R. W. Schoenlein, "Evidence for a Structurally-Driven Insulator-to-Metal Transition in VO_2: A View from The Ultrafast Timescale," *Physical Review B*, **70** (2004) 161102 (4).

[85] V. Eyert, "The Metal-Insulator Transitions of VO_2: A Band Theoretical Approach," *Annalen Der Physik*, **11** (2002) 650–704.

[86] M. W. Haverkort, Z. Hu, A. Tanaka, W. Reichelt, S. V. Streltsov, M. A. Korotin, V. I. Anisimov, H. H. Hsieh, H. J. Lin, C. T. Chen, D. I. Khomskii, and L. H. Tjeng, "Orbital-Assisted Metal-Insulator Transition in VO_2," *Physical Review Letters*, **95** (2005) 196404 (4).

[87] M. Pattanayak, M. N. F. Hoque, Y. C. Ho, W. Li, Z. Fan, and A. A. Bernussi, "Ultrahigh Tunability of Resistive Switching in Strongly Correlated Functional Oxide," *Applied Materials Today*, **30** (2023) 101642 (11).

[88] L. Chen, X. Wang, D. Wan, Y. Cui, B. Liu, S. Shi, H. Luo, and Y. Gao, "Energetics, Electronic and Optical Properties of X (X = Si, Ge, Sn, Pb) Doped VO_2 (M) from First-Principles Calculations," *Journal of Alloys and Compounds*, **693** (2017) 211–220.

[89] L. Chen, X. Wang, S. Shi, Y. Cui, H. Luo, and Y. Gao, "Tuning the Work Function of VO_2 (100) Surface by Ag Adsorption and Incorporation: Insights from First-Principles Calculations," *Applied Surface Science*, **367** (2016) 507–517.

[90] J. Jeong, N. Aetukuri, T. Graf, T. D. Schladt, M. G. Samant, and S. S. P. Parkin, "Suppression of Metal-Insulator Transition in VO_2 by Electric Field–Induced Oxygen Vacancy Formation," *Science*, **339** (2013) 1402–1405.

[91] C. Sun, L. Yan, B. Yue, H. Liu, and Y. Gao, "The Modulation of Metal–Insulator Transition Temperature of Vanadium Dioxide: A Density Functional Theory Study," *Journal of Materials Chemistry C*, **2** (2014) 9283–9293.

[92] M. Saeli, C. Piccirillo, I. P. Parkin, R. Binions, I. Ridley, "Energy Modelling Studies of Thermochromic Glazing," *Energy and Buildings*, **42** (2010) 1666–1673.

[93] F. Beteille, R. Morineau, J. Livage, and M. Nagano, "Switching Properties of $V_{1-x}Ti_xO_2$ Thin Films Deposited from Alkoxides," *Materials Research Bulletin*, **32** (1997) 1109–1117.

[94] S. C. Barron, J. M. Gorham, and M. L. Green, "Thermochromic Phase Transitions in VO_2-Based Thin Films for Energy-Saving Applications," *ECS Transactions*, **61** (2014) 387–393.

[95] S. C. Barron, J. M. Gorham, M. P. Patel, and M. L. Green, "High-Throughput Measurements of Thermochromic Behavior in $V_{1-x}Nb_xO_2$ Combinatorial Thin Film Libraries," *ACS Combinatorial Science*, **16** (2014) 526–534.

[96] Y. Li, S. Ji, Y. Gao, H. Luo, and M. Kanehira, "Core-Shell VO_2@TiO_2 Nanorods that Combine Thermochromic and Photocatalytic Properties for Application as Energy-Saving Smart Coatings," *Scientific Reports*, **3** (2013) 1370 (13).

[97] L. Q. Mai, B. Hu, T. Hu, W. Chen, and E. D. Gu, "Electrical Property of Mo-Doped VO2 Nanowire Array Film by Melting-Quenching Sol-Gel Method," *The Journal of Physical Chemistry B*, **110** (2006) 19083–19086.

[98] H. Zhang, Z. Wu, R. Niu, X. Wu, Q. He, and Y. Jiang, "Metal-Insulator Transition Properties of Sputtered Silicon-Doped and Undoped Vanadium Dioxide Films at Terahertz Range," *Applied Surface Science*, **331** (2015) 92–97.

[99] W. Zhang, K. Wang, L. Fan, L. Liu, P. Guo, C. Zou, J. Wang, H. Qian, K. Ibrahim, W. Yan, F. Q. Xu, and Z. Wu, "Hole Carriers Doping Effect on the Metal-Insulator Transition of N-Incorporated Vanadium Dioxide Thin Films," *The Journal of Physical Chemistry C*, **118** (2014) 12837–12844.

[100] A. Gentle, and G. Smith, "Dual Metal Insulator and Insulator Insulator Switching in Nanoscale and Al Doped VO_2," *Journal of Physics D: Applied Physics*, **41** (2008) 015402 (5).

[101] B. Chen, D. Yang, P. A. Charpentier, and M. Zeman, "Al^{3+}-Doped Vanadium Dioxide Thin Films Deposited by PLD," *Solar Energy Materials and Solar Cells*, **93** (2009) 1550–1554.

[102] M. Wan, M. Xiong, N. Li, B. Liu, S. Wang, W. Y. Ching, and X. Zhao, "Observation of Reduced Phase Transition Temperature in N-Doped Thermochromic Film of Monoclinic VO_2," *Applied Surface Science*, **410** (2017) 363–372.

[103] E. Gagaoudakis, I. Kortidis, G. Michail, K. Tsagaraki, V. Binas, G. Kiriakidis, and E. Aperathitis, "Study of Low Temperature RF-Sputtered Mg-Doped Vanadium Dioxide Thermochromic Films Deposited on Low-Emissivity Substrates," *Thin Solid Films*, **601** (2016) 99–105.

[104] S. Chen, J. Liu, L. Wang, H. Luo, and Y. Gao, "Unraveling Mechanism on Reducing Thermal Hysteresis Width of VO_2 by Ti Doping: A Joint Experimental and Theoretical Study," *The Journal of Physical Chemistry C*, **118** (2014) 18938–18944.

[105] N. Mlyuka, G. A. Niklasson, and C. G. Granqvist, "Mg Doping of Thermochromic VO_2 Films Enhances the Optical Transmittance and Decreases the Metal-Insulator Transition Temperature," *Applied Physics Letters*, **95** (2009) 171909 (3).

[106] J. Zhou, Y. Gao, X. Liu, Z. Chen, L. Dai, C. Cao, H. Luo, M. Kanahira, C. Sun, and L. Yan, "Mg-Doped VO_2 Nanoparticles: Hydrothermal Synthesis, Enhanced Visible Transmittance and Decreased Metal-Insulator Transition Temperature," *Physical Chemistry Chemical Physics*, **15** (2013) 7505–7511.

[107] J. Wan, Q. Ren, N. Wu, and Y. Gao, "Density Functional Theory Study of M-Doped (M = B, C, N, Mg, Al) VO_2 Nanoparticles for Thermochromic Energy-Saving Foils," *Journal of Alloys and Compounds*, **662** (2016) 621–627.

[108] I. Abdellaoui, G. Merad, M. Maaza, and H. S. Abdelkader, "Electronic and Optical Properties of Mg-, F-Doped and Mg\F-codoped M_1-VO_2 via Hybrid Density Functional Calculations," *Journal of Alloys and Compounds*, **658** (2016) 569–575.

[109] Z. Huang, C. Chen, C. Lv, and S. Chen "Tungsten-Doped Vanadium Dioxide Thin Films on Borosilicate Glass for Smart Window Application," *Journal of Alloys and Compounds*, **564** (2013) 158–161.

[110] Y. Ningyi, L. Jinhua, and L. Chenglu, "Valence Reduction Process from Sol–Gel V_2O_5 to VO_2 Thin Films," *Applied surface science*, **191** (2002) 176–180.

[111] T. Hanlon, J. Coath, and M. Richardson, "Molybdenum-Doped Vanadium Dioxide Coatings on Glass Produced by the Aqueous Sol–Gel Method," *Thin Solid Films*, **436** (2003) 269–272.

[112] W. Burkhardt, T. Christmann, S. Franke, W. Kriegseis, D. Meister, B. K. Meyer, W. Niessner, D. Schalch, and A. Scharmann, "Tungsten and Fluorine Co-Doping of VO_2 Films," *Thin Solid Films*, **402** (2002) 226–231.

[113] T. C. K. Yang, Y. L. Yang, R. C. Juang, T. W. Chiu, and C. C. Chen, "The Novel Preparation Method of High-Performance Thermochromic Vanadium Dioxide Thin Films by Thermal Oxidation of Vanadium-Stainless Steel Co-Sputtered Films," *Vacuum*, **121** (2015) 310–316.

[114] Y. Zhang, J. Zhang, X. Zhang, C. Huang, Y. Zhong, and Y. Deng, "The Additives W, Mo, Sn and Fe for Promoting the Formation of VO_2 (M) and Its Optical Switching Properties," *Materials Letters*, **92** (2013) 61–64.

[115] W. Li, S. Ji, K. Qian, and P. Jin, "Preparation and Characterization of VO_2 (M)-SnO_2 Thermochromic Films for Application as Energy-Saving Smart Coatings," *Journal of Colloid and Interface Science*, **456** (2015) 166–173.

[116] C. Liu, H. Wang, X. Zhanga, and D. Chen, "Morphology- and Phase-Controlled Synthesis of Monodisperse Lanthanide-Doped $NaGdF_4$ Nanocrystals with Multicolor Photoluminescence," *Journal of Materials Chemistry*, **19** (2009) 489–496.

[117] C. G. Granqvist, "Spectrally Selective Coatings for Energy Efficiency and Solar Applications," *Physica Scripta*, **32** (1985) 401.

[118] R. Lopez, L. A. Boatner, T. E. Haynes, R. F. Haglund, and L. C. Feldman, "Switchable Reflectivity on Silicon from a Composite VO_2-SiO_2 Protecting Layer," *Applied Physics Letters*, **85** (2004) 1410–1412.

[119] J. Zhou, Y. Gao, Z. Zhang, H. Luo, C. Cao, Z. Chen, L. Dai, and X. Liu, "VO_2 Thermochromic Smart Window for Energy Savings and Generation," *Scientific Reports*, **3** (2013) 3029 (5).

[120] A. A. Bugayev, and M. C. Gupta, "Femtosecond Holographic Interferometry for Studies of Semiconductor Ablation Using Vanadium Dioxide Film," *Optics Letters*, **28** (2003) 1463–1465.

[121] M. Soltani, M. Chaker, E. Haddad, R. V. Kruzelecky, and D. Nikanpour, "Optical Switching of Vanadium Dioxide Thin Films Deposited by Reactive Pulsed Laser Deposition," *Journal of Vacuum Science & Technology A Vacuum Surfaces and Films*, **22** (2004) 859–864.

[122] J. S. Chivian, W. E. Case, and D. H. Rester, "A 10.6 μm Scan Laser with Programmable VO_2 Mirror," *IEEE Joiurnal Quantum Electron*, **15** (1979) 1326–1328.

[123] C. Chen, and Z. Zhou, "Optical Phonons Assisted Infrared Absorption in VO_2 Based Bolometer," *Applied Physics Letters*, **91** (2007) 011107 (3).

[124] L. A. L. De Almeida, G. S. Deep, A. M. N. Lima, I. A. Khrebtov, V. G. Malyarov, and H. Neff, "Modeling and Performance of Vanadium-Oxide Transition Edge Microbolometers," *Applied Physics Letters*, **85** (2004) 3605–3607.

[125] A. Holsteen, I. S. Kim, and L. J. Lauhon, "Extraordinary Dynamic Mechanical Response of Vanadium Dioxide Nanowires around the Insulator to Metal Phase Transition," *Nano Letters*, **14** (2014) 1898–1902.

[126] K. Liu, C. Cheng, Z. Cheng, K. Wang, R. Ramesh, and J. Wu, "Giant-Amplitude, High-Work Density Microactuators with Phase Transition Activated Nanolayer Bimorphs," *Nano Letters*, **12** (2012) 6302–6308.

[127] M. J. Lee, Y. Park, D. S. Suh, E. H. Lee, S. Seo, D. C. Kim, R. Jung, B. S. Kang, S. E. Ahn, C. B. Lee, D. H. Seo, Y. K. Cha, I. K. Yoo, J. S. Kim, and B. H. Park, "Two Series Oxide Resistors Applicable to High Speed and High-Density Non-volatile Memory," *Advanced Materials*, **19** (2007) 3919–3923.

[128] M. Son, J. Lee, J. Park, J. Shin, G. Choi, S. Jung, W. Lee, S. Kim, S. Park, and H. Hwang, "Excellent Selector Characteristics of Nanoscale VO_2 For High-Density Bipolar ReRAM Applications," *IEEE Electron Device Letter*, **32** (2011) 1579–1581.

.

[129] T. Driscoll, H. T. Kim, B. G. Chae, M. D. Ventra, and D. N. Basov, "Phase-Transition Driven Memristive System," *Applied Physics Letters*, **95** (2009) 043503 (3).

[130] B. Wu, A. Zimmers, H. Aubin, R. Ghosh, Y. Liu, and R. Lopez, "Electric-Field-Driven Phase Transition in Vanadium Dioxide," *Physical Review B*, **84** (2011) 241410 (4).

[131] B. G. Chae, H. T. Kim, D. H. Youn, and K. Y. Kang, "Abrupt Metal-Insulator Transition Observed in VO_2 Thin Films Induced by a Switching Voltage Pulse," *Physica B: Condensed Matter*, **369** (2005) 76–80.

[132] C. Ko, and S. Ramanathan, "Observation of Electric Field-Assisted Phase Transition in Thin Film Vanadium Oxide in a Metal-Oxide-Semiconductor Device Geometry," *Applied Physics Letters*, **93** (2008) 252101 (4).

[133] D. Ruzmetov, G. Gopalakrishnan, C. Ko, V. Narayanamurti, and S. Ramanathan, "Three-Terminal Field Effect Devices Utilizing Thin Film Vanadium Oxide as the Channel Layer," *Journal of Applied Physics*, **107** (2010) 114516 (8).

[134] L. Chua, "Memristor-the Missing Circuit Element," *IEEE Transactions on Circuit Theory*, **18** (1971) 507–519.

[135] D. B. Strukov, G. S. Snider, D. R. Stewart, and R. S. Williams, "The Missing Memristor Found," *Nature*, **453** (2008) 80–83.

[136] Z. Wang, H. Wu, G. W. Burr, C. S. Hwang, K. L. Wang, Q. Xia, and J. J. Yang, "Resistive Switching Materials for Information Processing," *Nature Reviews Materials*, **5** (2020) 173–195.

[137] Y. Zhang, Z. Wang, J. Zhu, Y. Yang, M. Rao, W. Song, Y. Zhuo, X. Zhang, M. Cui, L. Shen, R. Huang, J. J. Yang, "Brain Inspired Computing with Memristors: Challenges in Devices, Circuits, and Systems," *Applied Physics Reviews*, **7** (2020) 011308 (24).

[138] C. Li, Z. Wang, M. Rao, D. Belkin, W. Song, H. Jiang, P. Yan, Y. Li, P. Lin, M. Hu, N. Ge, J. P. Strachan, M. Barnell, Q. Wu, R. S. Williams, J. J. Yang and Q. Xia, "Long Short-Term Memory Networks in Memristor Crossbar Arrays," *Nature Machine Intelligence*, **1** (2019) 49–57.

[139] N. K. Upadhyay, W. Sun, P. Lin, S. Joshi, R. Midya, X. Zhang, Z. Wang, H. Jiang, J. H. Yoon, M. Rao, M. Chi, Q. Xia, and J. J. Yang, "A Memristor with Low Switching Current and Voltage for 1S1R Integration and Array Operation," *Advanced Electronic Materials*, **6** (2020) 1901411 (9).

[140] H. Jiang, K. Yamada, Z. Ren, T. Kwok, F. Luo, Q. Yang, X. Zhang, J. J. Yang, Q. Xia, Y. Chen, H. Li, Q. Wu, and Mark Barnell, "Pulse-Width Modulation Based Dot-Product Engine for Neuromorphic Computing System Using Memristor Crossbar Array," *IEEE International Symposium on Circuits and Systems (ISCAS)*, (Florence, Italy) (2018) 1–4.

[141] X. Yan, Z. Zhou, J. Zhao, Q. Liu, H. Wang, G. Yuan, and J. Chen, "Flexible Memristors as Electronic Synapses for Neuro-Inspired Computation Based on Scotch Tape-Exfoliated Mica Substrates," *Nano Research*, **11** (2018) 1183–1192.

[142] X. Xu, P. Sharma, S. Shu, T. S. Lin, P. Ciais, F. N. Tubiello, P. Smith, N. Campbell and A. K. Jain, "Global Greenhouse Gas Emissions from Animal-Based Foods are Twice those of Plant-Based Foods," *Nature Food*, **2** (2021) 724–732.